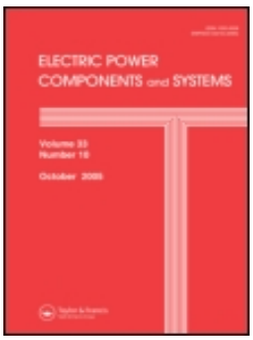

Taylor & Francis
Taylor & Francis Group

Electric Power Components and Systems

ISSN: 1532-5008 (Print) 1532-5016 (Online) Journal homepage: https://www.tandfonline.com/loi/uemp20

Dynamic Performance of Microturbine Generation System Connected to a Grid

D. N. Gaonkar , G. N. Pillai & R. N. Patel

To cite this article: D. N. Gaonkar , G. N. Pillai & R. N. Patel (2008) Dynamic Performance of Microturbine Generation System Connected to a Grid, Electric Power Components and Systems, 36:10, 1031-1047, DOI: 10.1080/15325000802046587

To link to this article: https://doi.org/10.1080/15325000802046587

Electric Power Components and Systems, 36:1031–1047, 2008

ISSN: 1532-5008 print/1532-5016 online
DOI: 10.1080/15325000802046587

Taylor & Francis
Taylor & Francis Group

Dynamic Performance of Microturbine Generation System Connected to a Grid

D. N. GAONKAR,[1] G. N. PILLAI,[2] and R. N. PATEL[2]

[1]Department of Electrical Engineering, National Institute of Technology Karnataka, Surathkal, Mangalore (D.K.), Karnataka, India
[2]Department of Electrical Engineering, Indian Institute of Technology Roorkee, Roorkee, Uttaranchal, India

Abstract *The interconnection of distribution generation systems into distribution networks has great impact on real-time system operation, control, and planning. It is widely accepted that microturbine generation (MTG) systems are currently attracting a lot of attention to meet customers' needs in the distributed power generation market. In order to investigate the performance of MTG systems, their efficient modeling is required. This article presents the dynamic model of an MTG system, suitable for grid connection to study the performance of the MTG system. The presented model uses back-to-back power electronic converter topology for grid connection, which allows the bidirectional power flow between the grid and MTG system. Thus, the need of separate starting arrangements during launching of the microturbine is avoided. The components of the system are built from the dynamics of each part with their interconnections. The dynamics of the model have been studied under various grid disturbance conditions. The converter control strategies for MTG system operation in grid-connected mode are presented in this article. This article also compares the various grid connection topologies suitable for MTG system interconnection. The simulation results show that the developed model performance is not affected by the grid disturbances considered in the study, and that it has the ability to adjust the supply as per the power requirements of the load within the MTG system rating.*

Keywords distributed generation, MTG system, permanent magnet synchronous generator, grid connection, voltage unbalance

1. Introduction

The deregulation of electric power utilities, advancement in technology, environmental concerns, and emerging power markets are leading to increased interconnection of distributed generators to the utility system. This is leading to the integration of a large number of distribution generation (DG) systems to utility network. The DG systems can be based on renewable technologies, such as wind turbine, photovoltaic, or recent promising non-renewable technologies such as microturbine and fuel cell. Small DG

Received 8 February 2007; accepted 18 February 2008.
Address correspondence to Prof. D. Gaonkar, Department of Electrical Engineering, National Institute of Technology Karnataka, Surathkal, Mangalore (D.K.), Karnataka, 575 025 India. E-mail: dngaonkar@nitk.ac.in

systems based on microturbine technology with a capacity smaller than 500 kW are gaining popularity among industry and utilities in the last few years due to their higher operating efficiencies, lower emission levels, and low initial cost [1]. The microturbine generation (MTG) systems are more reliable and lightweight, can operate with different fuels, and are proving to be a supplement to the traditional forms of power generation, whether it is stationary, mobile, remote, or interconnected with the utility applications.

Once connected to the power distribution system, these generators will affect the dynamics of the system, and their transient behavior can be assessed only if a detailed nonlinear dynamic model is used. Thus, an accurate model of the MTG system is required to analyze the factors (such as transient response, stability, power quality including harmonics, voltage regulation, and protection) when connected to the distribution network [2]. Until now, few works were undertaken on the modeling, simulation, and control of the MTG systems, even though microturbine is based on gas-turbine technology, which is well established. Also there is a lack of adequate information on the performance of the MTG systems. The power electronic converter interface is needed for connecting a single-shaft MTG system to utility or customer load. This presents a significant challenge in modeling power electronic converter controls to provide increased functionalities under various network conditions for better performance [3]. The dynamic model of the MTG system for isolated operation is presented in [4–6]. In these references, a combustion gas-turbine model (presented in [7]) is used to model the microturbine and topology of passive rectifier, and an inverter with a DC link is used to interface the MTG system to the utility. A simplified transfer function model of the turbine and governor is used to model the MTG system [8].

A grid-connected model of the MTG system with matrix converter and AC-DC-AC converters are reported [9, 10] for the evaluation of the electromagnetic transients of the MTG system. In these studies, a thermodynamic model of the microturbine is proposed, and PSCAD/EMTDC software is used for simulation. The performance of the reduced-order model of the MTG system, based on auto-regression with the exogenous (ARX) signal identification algorithm, is compared with the full model when connected to distribution feeders in [11]. Modeling of power electronic converter interface for grid connection of the MTG system with bidirectional power flow between the MTG system and grid is considered in [12]. The grid-side converter uses the instantaneous current-control-based pulse width modulation (PWM) with DC-voltage control. Simulation results of the performance of the modeled MTG system are validated with actual system operation [12].

This article presents a single-shaft MTG system model developed in Simulink of the MATLAB. The developed model considers the bidirectional power flow between the grid and MTG system with back-to-back converter topology. The grid-side converter uses the two-loop controller structure—a fast inner current control loop and a slow outer DC-link voltage-control loop. The independent control of dq components of the currents are done through decoupling for both machine- and grid-side converters. Extensive simulation is carried out to study the performance of the model when connected to the distribution network. The work also discusses the merits and demerits of various grid connection topologies for the MTG system.

2. MTG Systems

Two types of microturbine designs are available. One is the high-speed single-shaft design with the compressor and turbine mounted on the same shaft as the permanent

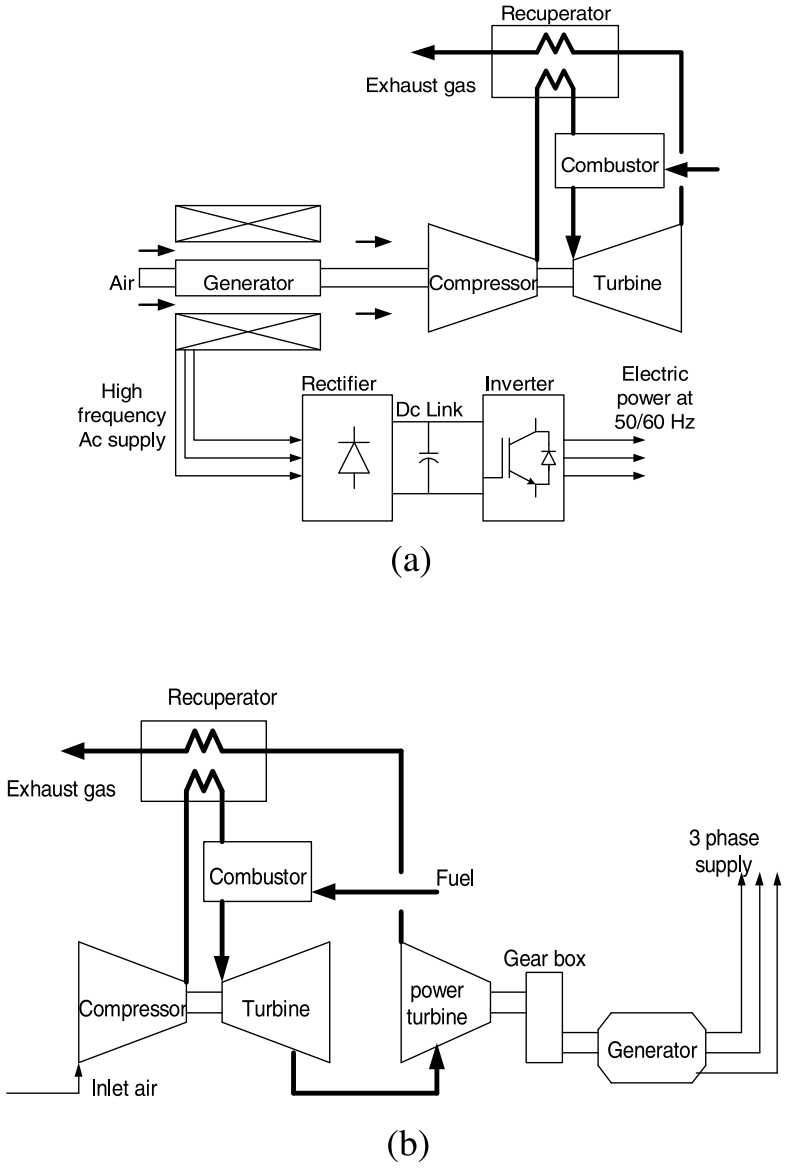

Figure 1. Schematic diagram of: (a) single-shaft MTG system and (b) split-shaft MTG system.

magnet synchronous generator, as shown in Figure 1(a). The generator generates power at very high frequency ranging from 1500 to 4000 Hz. The high-frequency voltage is first rectified and then inverted to a normal 50- or 60-Hz voltage. Another is the split-shaft design that has a power turbine rotating at 3600 rpm, and a conventional generator (usually an induction generator) connected via a gearbox, as shown in Figure 1(b). The power electronic interfacing is not required in this design. In both designs, along with the turbine, there are control systems, namely speed and acceleration control, fuel-flow control, and temperature control. The recuperator increases the efficiency of the microturbine by transferring heat from hot exhaust gases to the compressed air that is

fed to the combustion chamber. The MTG system can generate power in the range of 25 kW to 500 kW, and its efficiency for combined heat and power (CHP) application can go above 80% [1].

There are different topologies available for connecting the single-shaft MTG system to the grid. Figure 1(a) shows the passive rectifier and inverter combination with the DC link, and this topology needs a separate startup inverter to launch the microturbine. A cycloconverter or a matrix converter, shown in Figures 2(a) and 2(b), respectively, can be used to interface the microturbine generator to the grid [9, 13]. These converters directly

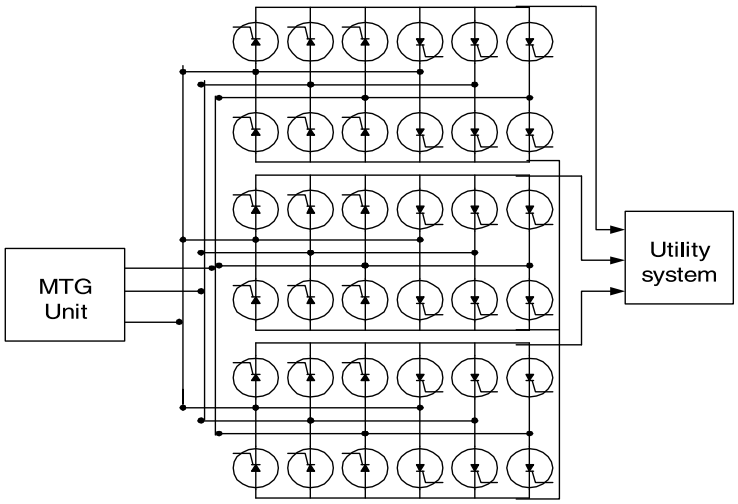

(a)

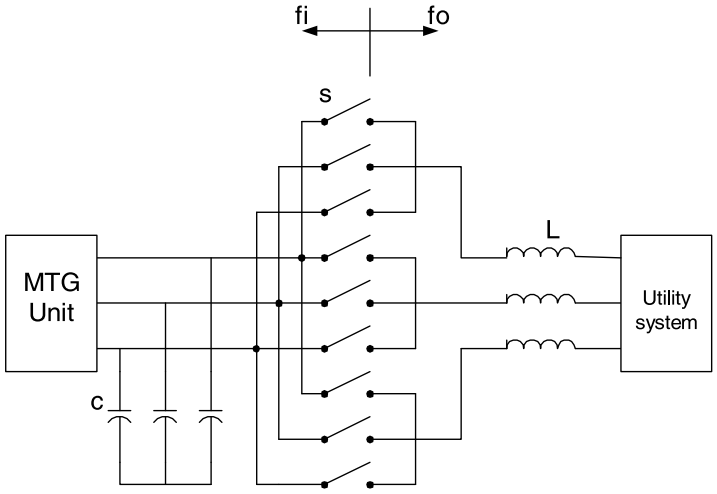

(b)

Figure 2. (a) Cycloconverter interface model and (b) matrix converter interface model.

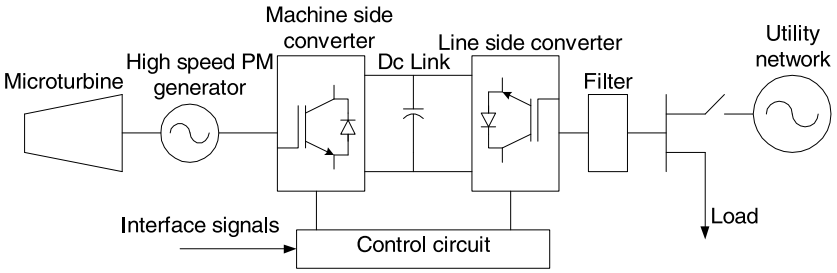

Figure 3. MTG system with back-to-back converter interface.

convert AC voltages at one frequency to AC voltages at another frequency with variable magnitude. For this reason, they are also called frequency changers. The disadvantages of these converters are that they have double the number of switches compared to the DC-link approach, and energy storage is not possible. Without energy storage in the converter, any fluctuations at either side of the converter will directly influence the other side.

The matrix converter can be used at a lower frequency than the PWM-based converters. Some advantages of the matrix converters are less thermal stress on the semiconductors and absence of the DC-link capacitors, which may increase the efficiency and life time. The drawbacks are the intrinsic limitation of the output voltage, the unavailability of true bidirectional switches, and the lack of decoupling between the input and output of the converter (as in the case of the back-to-back converter), and these may lead to some instability issues [3].

The configuration presented in this article uses back-to-back voltage-source converters (VSCs), as shown in Figure 3. This topology allows bidirectional power flow between the converter and grid, and hence, no separate starting arrangement is required. When starting, the permanent magnet synchronous machine (PMSM) acts as a motor and draws power from the grid to bring the turbine to a certain speed. In this mode, the line-side converter acts as a controlled rectifier, and the machine-side converter acts as an inverter and provides AC supply to the motor. During the generating mode, the PMSM acts as a generator and power flows from the MTG system to the grid. The machine-side and line-side converters act as a controlled rectifier and inverter, respectively. In both modes of operation, the grid-side converter regulates the DC-bus voltage, while the machine-side converter controls the PMSM speed and displacement factor.

3. Modeling of MTG System Components

3.1. Microturbine

A simplified single-shaft microturbine, including its control systems, is implemented in Simulink of the MATLAB and shown in Figure 4. In this article, the model presented in [7] has been implemented in Simulink of the MATLAB. The model consists of fuel control, turbine dynamics, and speed governor blocks. In this work, the electromechanical behavior of the MTG is the main interest. Thus, the recuperator is not included in the model, as it only serves to increase the turbine efficiency. Also, due to the recuperator's very slow response time, it has little influence on the timescale of our dynamic simulation. The speed controller operates on the speed error formed between the reference speed (one per unit) and speed of the PMSM [14]. Speed control is usually modeled by using a lead

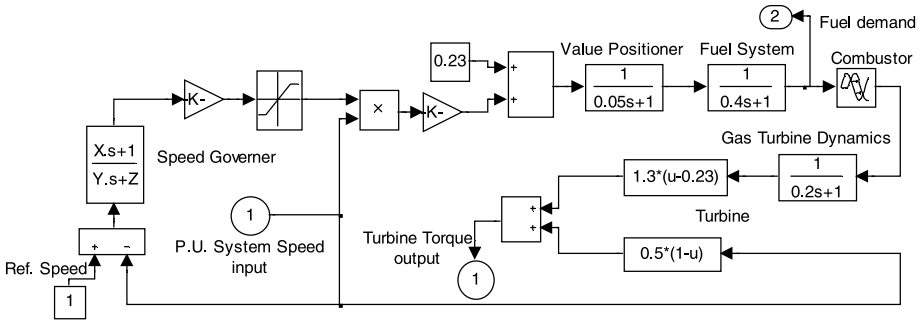

Figure 4. Simulink model of the microturbine.

lag transfer function or by a proportional-integral-derivative (PID) controller [15]. In this work, a lead lag transfer function has been used to represent the speed controller.

The governor-control parameters (shown in Figure 4) can be adjusted such that it can act with droop or as an isochronous governor. The temperature and acceleration controls are not included in the model and can be found in [6]. The per-unit value of the fuel demand signal directly corresponds to the per-unit value of mechanical power on the turbine base in steady state. The fuel-flow control system consists of a series of blocks including the valve position and flow dynamics. The fuel system positioner and actuator are represented in Eqs. (1) and (2).

The valve positioner equation:

$$e_1 = \frac{1}{0.05s + 1} F_d. \tag{1}$$

The fuel system actuator equation:

$$w_f = \frac{1}{0.4s + 1}. \tag{2}$$

Turbine torque:

$$T = 1.3(w_f - 0.23) + 0.5(\Delta\omega), \tag{3}$$

where F_d is the input to the fuel system, and w_f is the output of the fuel system. The valve positioner input signal e_1 is scaled by the gain value of 0.77 and offset by a value, which is the fuel flow, at no-load and at rated speed condition. The time delay after the fuel-flow control represents the delay in the governor control, using digital logic in place of analog devices. The fuel burned in the combustor results in turbine torque. The turbine torque is given in Eq. (3), where $\Delta\omega$ is the change in per-unit speed. The fuel flow at no-load is 23% and rises to 100% at the rated load. The model parameters given in [14] are used in this work.

3.2. PMSM

The PMSM drive is modeled with an assumption of sinusoidal-distributed windings and neglecting saturation, eddy currents, and hysteresis losses [16]. With these assumptions,

the stator dq equations of the PMSM in the rotor reference frame are

$$v_d = R_s i_d + L_d \frac{di_d}{dt} - \omega_r L_q i_q, \tag{4}$$

$$v_q = R_s i_q + L_q \frac{di_q}{dt} + \omega_r L_d i_d + w_r \lambda_m, \tag{5}$$

where

the stator resistance is denoted by R_s;
the d-axis and q-axis inductances are L_d and L_q, respectively;
ϕ_m is the flux linkage due to the permanent magnets; and
v_d and v_q are the dq-axis voltages.

In the dq-frame, the expression for electro-dynamic torque becomes

$$T_e = 1.5p(\lambda_m i_q + (L_d - L_q) i_q i_d). \tag{6}$$

The equation for motor dynamics can be given as

$$\frac{d}{dt}\omega_r = \frac{1}{J}(T_e - F\omega_r - T_M), \tag{7}$$

$$\frac{d}{dt}\theta_r = \omega_r, \tag{8}$$

where

p is the number of pole pairs,
T_e is the electromagnetic torque,
F is the combined viscous friction of the rotor and load,
ω_r is the rotor speed,
J is the moment of inertia,
θ_r is the rotor angular position, and
T_m is the shaft mechanical torque.

The d and q variables are obtained from the a, b, and c variables through Park's transformation given in Eq. (9), and the a, b, and c variables are obtained from the d and q variables through the inverse of Park's transformation as given in Eq. (10):

$$\begin{bmatrix} v_q \\ v_d \\ v_0 \end{bmatrix} = \frac{2}{3} \begin{bmatrix} \cos\theta_r & \cos(\theta_r - 120) & \cos(\theta_r + 120) \\ \sin\theta_r & \sin(\theta_r - 120) & \sin(\theta_r + 120) \\ 1/2 & 1/2 & 1/2 \end{bmatrix} \begin{bmatrix} v_a \\ v_b \\ v_c \end{bmatrix}, \tag{9}$$

$$\begin{bmatrix} v_a \\ v_b \\ v_c \end{bmatrix} = \begin{bmatrix} \cos\theta_r & \sin\theta_r & 1 \\ \cos(\theta_r - 120) & \sin(\theta_r - 120) & 1 \\ \cos(\theta_r + 120) & \sin(\theta_r + 120) & 1 \end{bmatrix} \begin{bmatrix} v_q \\ v_d \\ v_0 \end{bmatrix}. \tag{10}$$

3.3. Machine-side Converter Control

Figure 5 shows the high-efficiency drive control system for the MTG system. The commanded speed ω_{ref} is pre-calculated according to the turbine output power and is set to the optimum speed [17]. Based on the speed error, the commanded q-axis reference current i_{qref} is determined through the speed controller. In this system, the following proportional-integral (PI) controller is employed as the speed controller:

$$i_{qref} = K_{P\omega} e_\omega + K_{I\omega} \int e_\omega dt, \tag{11}$$

where $K_{P\omega}$ and $K_{I\omega}$ are the proportional and integral gains of the speed controller, respectively, while e_ω is the error between the reference speed and measured speed. The commanded optimal d-axis current i_{dref} is obtained from the maximum allowed phase-voltage and phase-current constraints of the drive, which are given in Eqs. (12) and (13). These constraints depend upon the machine rating and DC-link voltage.

$$v_d^2 + v_q^2 \leq V_{\max}^2, \tag{12}$$

$$i_d^2 + i_q^2 \leq I_{\max}^2. \tag{13}$$

Using the above constraints, and neglecting the voltage drop due to the stator resistance, the optimal d-axis current for a non-salient PMSM ($L_d = L_q$) can be obtained as

$$I_d = \frac{\frac{V_{\max}^2}{\omega^2} - L_q^2 I_{\max}^2 - \lambda_m^2}{2L_d \lambda_m}. \tag{14}$$

Considering the relationship $I_{\max}^2 = i_d^2 + i_q^2$, the optimal d-axis current can be given as a function of the q-axis current i_q, as

$$i_d = -\frac{\lambda_m}{L_d} + \sqrt{\left(\frac{V_{\max}}{\omega L_d}\right)^2 - \left(\frac{L_q}{L_d} i_q\right)^2}. \tag{15}$$

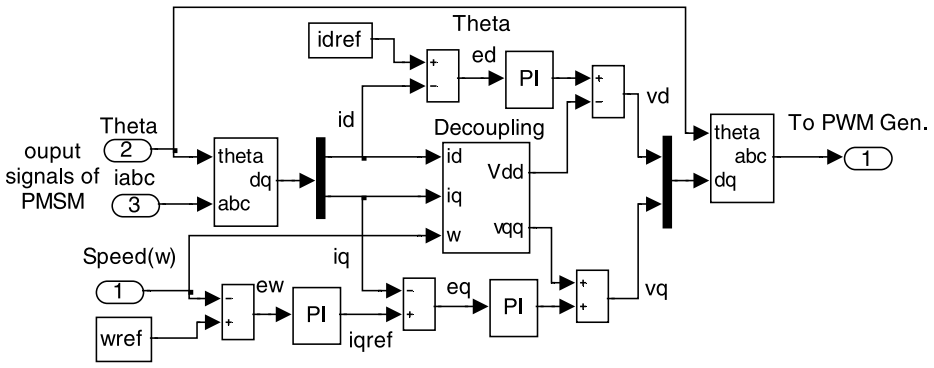

Figure 5. Machine-side converter controller.

Based on the current errors, the dq-axis reference voltages are determined by PI controllers, given as

$$v_d = K_{Pi} e_{id} + K_{Ii} \int e_{id} dt - \omega_r L_q i_q, \tag{16}$$

$$v_q = K_{Pi} e_{iq} + K_{Ii} \int e_{iq} dt + \omega_r (L_d i_d + \lambda_m), \tag{17}$$

where K_{Pi} and K_{Ii} are the proportional and integral gains of the controller, respectively; $e_{id} = i_{dref} - i_d$ is the d-axis current error; and $e_{iq} = i_{qref} - i_q$ is the q-axis current error. The decoupling terms $(-\omega_r L_q i_q)$ and $(\omega_r (L_d i_d + \lambda_m))$ are used in Eqs. (16) and (17), respectively, for the independent control of the d- and q-axis currents. The commanded dq-axis voltages (v_d, v_q) are transformed into a, b, and c variables (v_a, v_b, and v_c) and given to the PWM generator to generate the gate pulse for the machine-side converter.

3.4. Grid-side Converter Control

The objective of the grid-side converter is to keep the DC-link voltage constant, regardless of the magnitude and direction of the rotor power. A vector-control approach is used, with the reference frame oriented along the stator (or supply) voltage vector position, enabling independent control of the active and reactive power flowing between the supply and grid-side converter. The controllers of the grid-side VSC will be obtained with respect to Figure 6. Three phase voltages at the grid-side terminals of the converter are given as

$$v_{an} = L_f \frac{di_a}{dt} + R_f i_a + v_{gan}, \tag{18}$$

$$v_{bn} = L_f \frac{di_b}{dt} + R_f i_b + v_{gbn}, \tag{19}$$

$$v_{cn} = L_f \frac{di_c}{dt} + R_f i_c + v_{gcn}, \tag{20}$$

where L_f and R_f are the filter inductance and resistance, respectively. Using Park's transformation, Eqs. (18)–(20) can be transformed to the dq-reference frame. The resulting

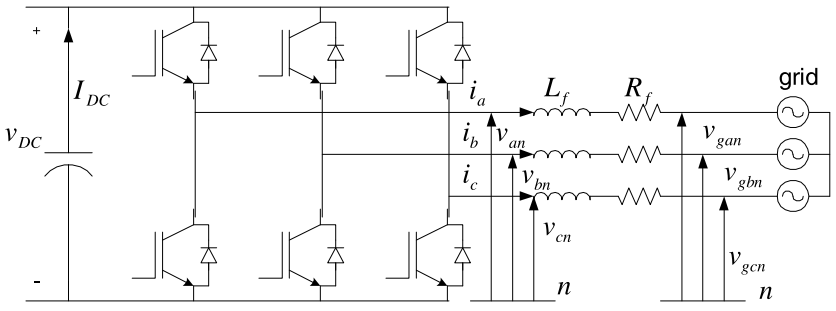

Figure 6. Grid-side VSC.

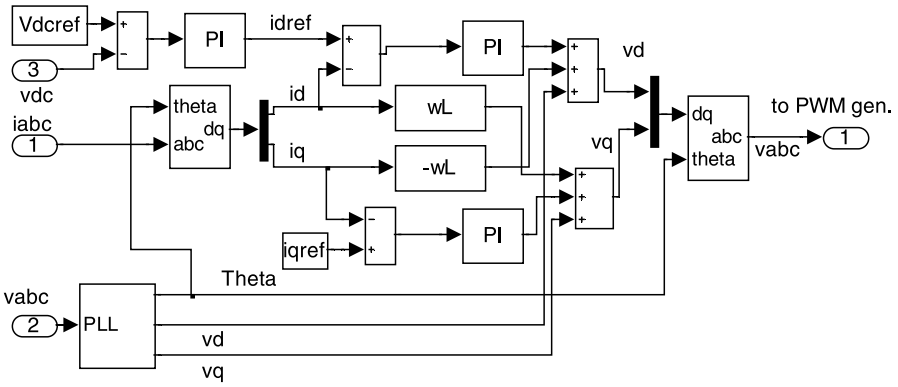

Figure 7. Grid-side converter controller.

voltage equations in the dq reference frame are given as

$$v_d = L_f \frac{di_d}{dt} + R_f i_d - \omega L_f i_q + v_d, \tag{21}$$

$$v_q = L_f \frac{di_q}{dt} + R_f i_q + \omega L_f i_d + v_q. \tag{22}$$

The control structure for the grid-connected mode of operation of the MTG system is implemented using Eqs. (21) and (22) along with the DC voltage controller, as shown in Figure 7. The standard PI controllers are used to regulate the currents in the dq synchronous frame in the inner control loop. Another PI controller is used in the outer loop to regulate the capacitor voltage in accordance with the current to be injected into the grid. Its output is the reference for the active current PI controller. In order to obtain only transfer of active power, the i_q current reference is set to zero. Also, to have an independent control of the current components i_d and i_q, the decoupling voltage components are added to output of the PI current controllers.

4. Simulation and Results

Figure 8 shows the simulation model implemented in the SimPowerSystems of the MATLAB to study the performance of the MTG system operation in grid-connected mode. The utility network, to which the MTG system is connected, is represented by a three-phase sinusoidal source with its impedance. The series resistor and inductor (RL) filter is used at the grid side of the MTG system.

The simulation parameters of the model are given in Table 1. The microturbine generation system takes per-unit speed of the PMSM as input. The torque output of the microturbine is given as an input mechanical torque (T_m) to the PMSM. The direction of the torque T_m is positive during the motoring mode and made negative during generating mode of the PMSM. The machine-side converter controller takes the rotor-angle speed and three phase stator current signals of the PMSM as inputs. In all presented cases, the voltage across the capacitor is zero at the start of simulation.

During the start up, the PMSM operates as a motor to bring the turbine to a speed of 30,000 rpm. In this case, power flows from the grid to the MTG system. Figure 9(a) shows that the microturbine reaches the set value of speed in 0.4 sec. At this speed, the

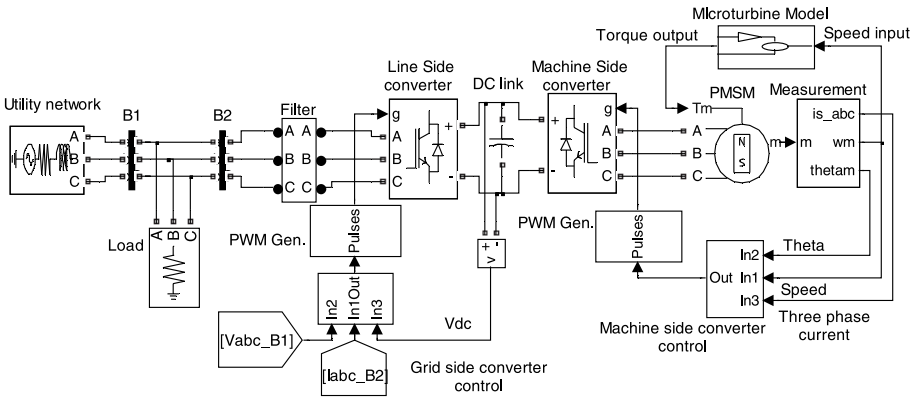

Figure 8. MATLAB/SimPowerSystems implementation of MTG system connected to grid.

MTG system absorbs power of 5.4 kW, as shown in Figure 9(b). The PMSM terminal voltage reaches 192 V at a frequency of 500 Hz at this speed. To ensure this operating condition at a unity displacement factor, the pre-calculated reference speed and direct current component i_d are set to 3142 rad/sec and -5.36 A, respectively [18]. The speed regulator provides the reference for the i_q current component.

At $t = 0.4$ sec, the sign of the PMSM input torque is changed to operate in generating mode. The power starts flowing from the MTG system to the grid, as shown in Figure 9(b). At $t = 0.4$ sec, the reference speed and i_d current are set to the pre-calculated values of 5849 rad/sec and -15.89 A in order to generate power of 14 kW. In order to study the performance of the MTG system model for the change in power, the reference values of speed and i_d current component are again changed at $t = 1.3$ sec to generate the rated power of 28 kW. When PMSM generates 28 kW, its line-to-line voltage and fundamental root mean square (RMS) output current reach the value of 480 V and 33.84 A, respectively. Figure 9(c) shows that the reactive power injected to the grid during the simulation period is zero.

Figure 10(a) shows the variation of electromagnetic torque of the PMSM. It can be observed that the change in the operation mode of the PMSM in simulation is instantaneous. But this may not be the same in practicality because of the inertia of the machine. Figure 10(b) shows the nature of the stator current waveform of the PMSM.

Table 1
Simulation parameters for the model shown in Figure 8

Grid parameters	480 V, 60 Hz, $R_s = 0.4\ \Omega$ and $L_s = 2$ mH
Filter parameters	$L = 0.97$ mH, $R = 0.21\ \Omega$
Switching frequency	Grid-side converter = 8 Khz
	Machine-side converter = 20 KHz
DC-link capacitance	5000 μF
PI controllers sampling time	100 μsec
PMSM parameters	480 V, 30 kW, 1.6 KHz, 96,000 rpm
	$R_s = 0.25\ \Omega$, $L_q = L_d = 0.0006875$ H
Microturbine parameters	Gain(K) = 25, $X = 0.4$, $Y = 0.05$, and $Z = 1$

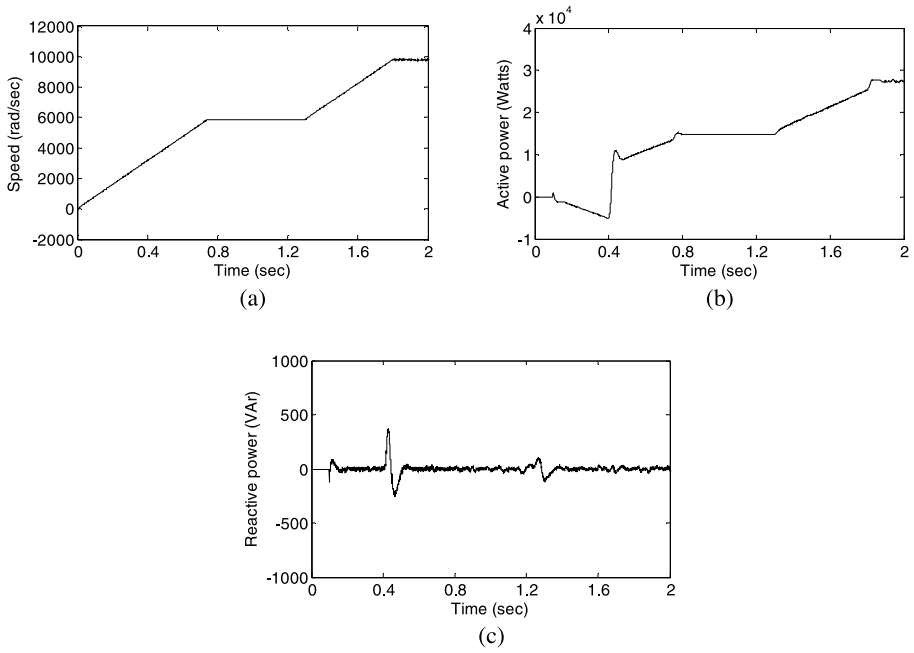

Figure 9. Motoring and generating operation of PMSM: (a) speed variation of PMSM, (b) active power variation at the grid side of the MTG system, and (c) reactive power variations at the grid side of the MTG system.

It can be observed from Figure 10(c) that the DC-link voltage is regulated to 760 V by the grid-side converter [19].

Figures 10(d) and 10(e) show the variation of the i_d component of the injected-grid current and the voltage across the terminals of the load. There is a small decrease in the voltage for $t < 0.4$ sec, as shown in Figure 10(e). This is due to the increasing power drawn by the MTG system during motoring-mode operation as, shown in Figure 9(b). In motoring mode, both the MTG system and the load draw power from the grid. The total harmonic distortion (THD) of the voltage is about 2.3% during the entire simulation time, as shown in Figure 10(f).

4.1. Response of the MTG Model for Various Disturbances in the Grid

Simulations are carried out to study the performance of the developed model of the MTG system under various disturbances originating from the grid. Three grid disturbance conditions are considered for study. They are balanced voltage dip, unbalanced voltage, and harmonic distortion in the grid voltage. In all these conditions, the MTG system is operated to deliver 28 kW.

4.1.1. Balanced Voltage Dips. The simulation results in Figure 11 show the performance of the MTG system under balanced grid voltage dip. At $t = 1.4$ to 1.5sec (10 cycle), 20% balanced voltage dip is introduced in the grid, as seen from Figure 11(a). The variation of the injected reactive power due to the balanced dip is regulated to zero by the grid-side converter controller, as shown in Figure 11(b). Figures 11(c), 11(d),

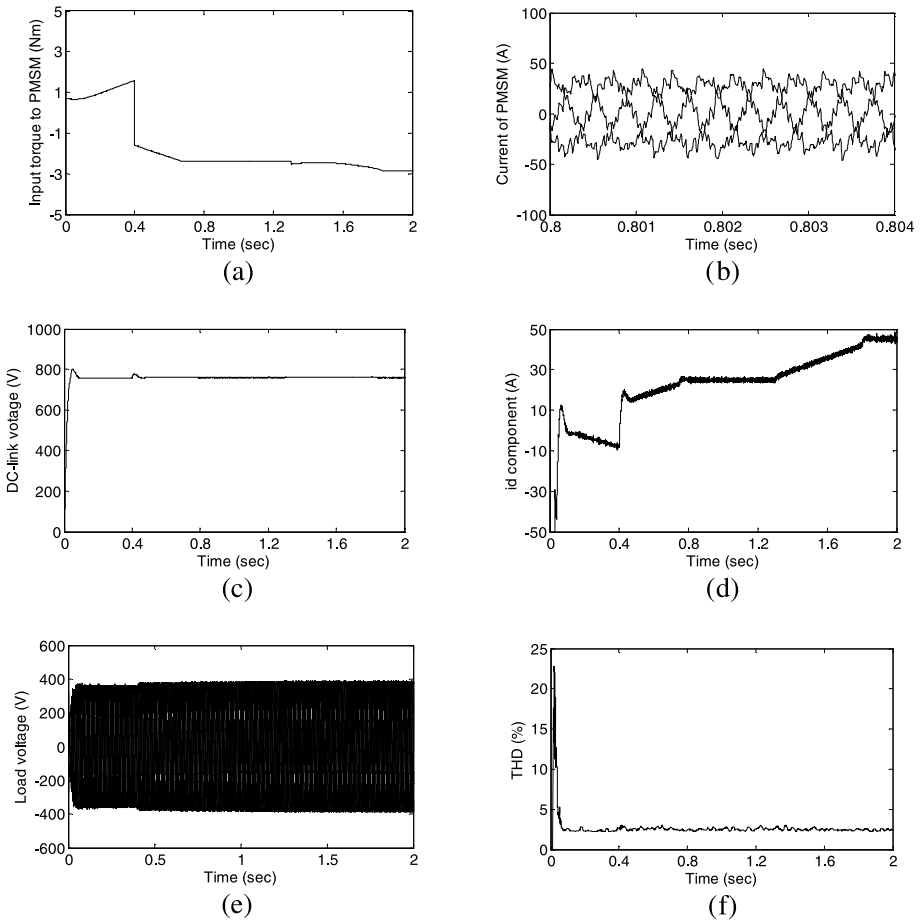

Figure 10. (a) Electromagnetic torque variations of the PMSM, (b) detailed variations of the stator current of PMSM, (c) DC-link voltage variation, (d) i_d component of the injected-grid current, (e) line-to-line voltage at the load terminals, and (f) percentage of THD variation at the load terminals.

and 11(e) show the variation in the active power output of the MTG system and the i_q and i_d components of the injected current to the grid, respectively.

4.1.2. Voltage Unbalance. At $t = 1.4$ sec, the voltage unbalance in the grid is introduced by creating a short-circuit fault between phase A and ground. Thus, the phase A voltage is reduced by 20% of its nominal value. In this case, it is assumed that unbalance exist until the end of the simulation time. The simulated phase voltage of the grid is shown in Figure 12(a). At the point of voltage unbalance, reactive power injected to the grid suddenly increases and then is regulated to zero, as seen in Figure 12(b). The active power injected to the grid is not affected by the unbalance in the grid voltage, as observed in Figure 12(c). There is no variation in the i_d and i_q components of the injected-grid current during unbalance in the grid voltage, as shown in Figures 12(d) and 12(e). During this unbalance, phase A current increases to keep the active power output of the MTG system constant.

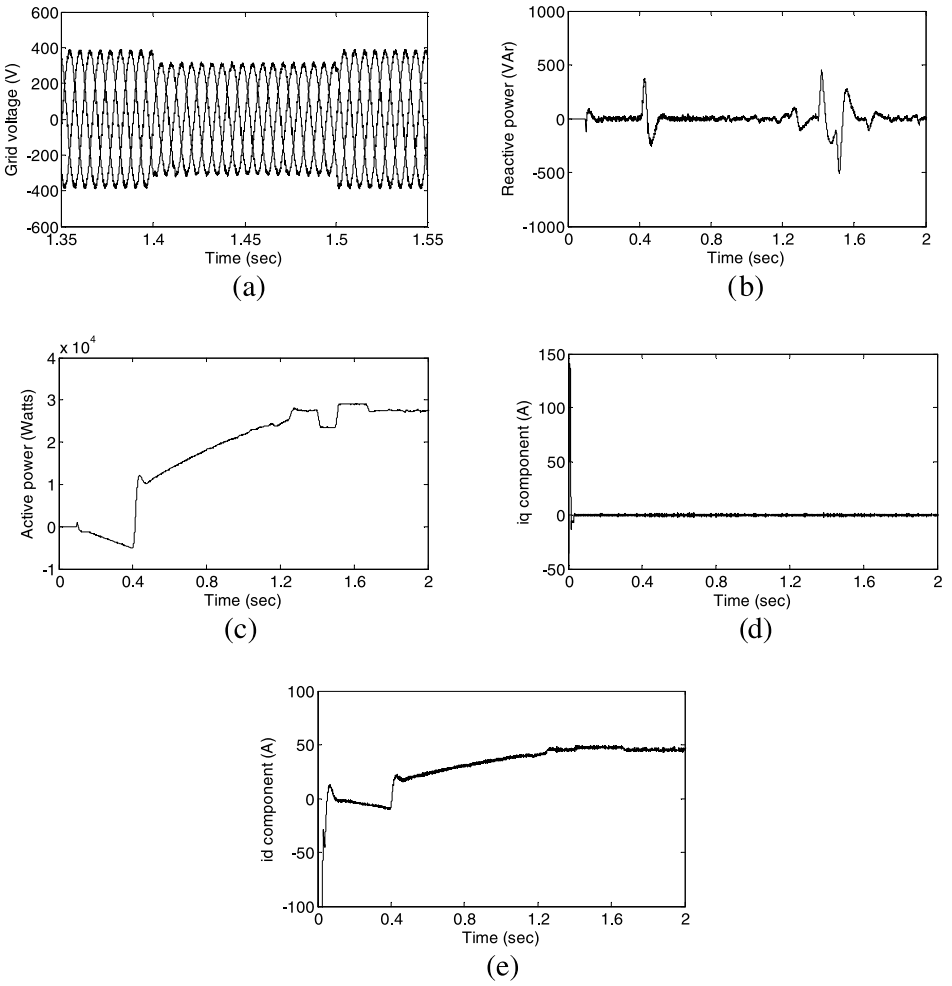

Figure 11. Response of MTG system for balanced voltage dip in the grid: (a) balanced voltage dip in line-to-line grid voltage, (b) reactive power exchanged with grid, (c) the injected active power to the grid, (d) i_q component of the injected current, and (e) i_d component of the injected current to the grid.

4.1.3. Polluted Grid Voltage. The simulation results in Figure 13 show the performance of the MTG system under harmonic-polluted grid voltages. The various non-linear loads connected to the grid are the main cause for the harmonic pollution in the grid voltage. In order to study the performance of the model under polluted-grid voltage, along with the fundamental component, 10% of the fifth and 6% of the seventh harmonics are injected to the grid. The polluted-grid voltages under this condition are shown in Figure 13(a). As per IEEE Standard 1547-2003 [20], the THD at the point of common coupling to the grid should be kept below 5%, but in this case, it varies from 10 to 8%, as shown in Figure 13(b). Figures 13(c) and 13(d) show the variation of reactive power exchanged with the grid and injected active power, respectively. The variation of the dq component of the injected line currents is shown in Figures 13(e) and 13(f), respectively.

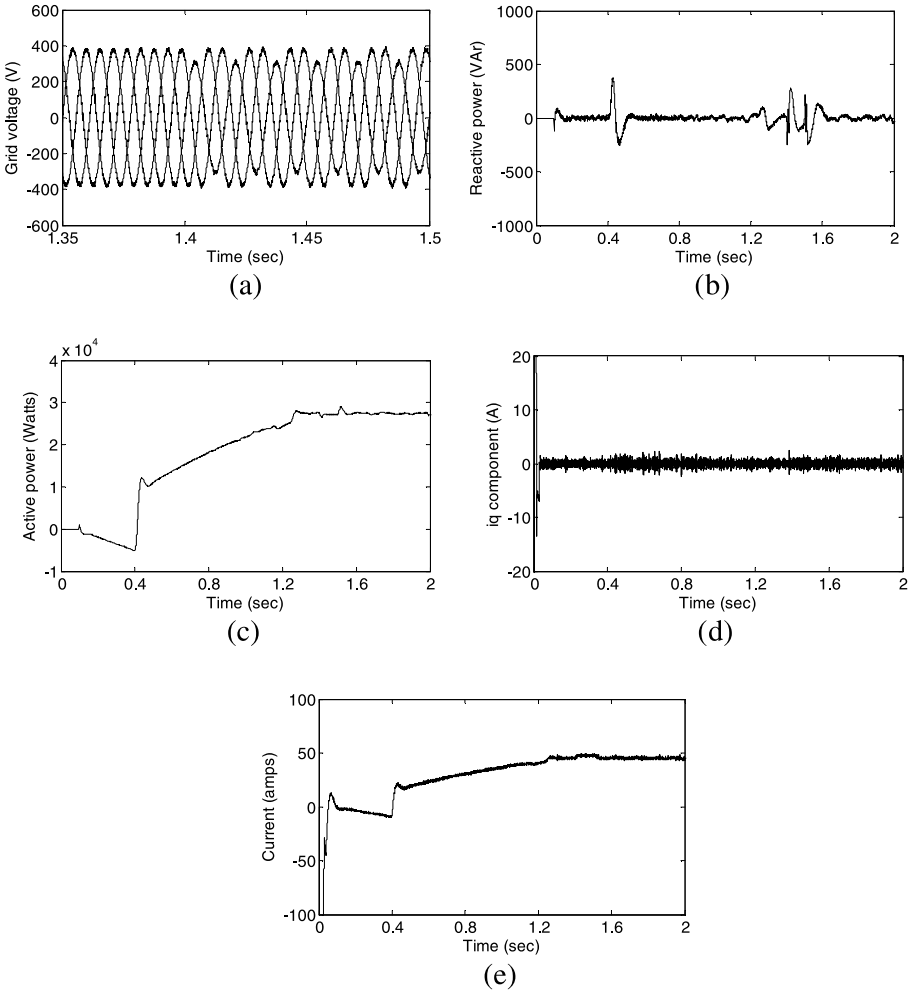

Figure 12. Response of MTG system for voltage unbalances in the grid: (a) unbalanced phase voltage of the grid, (b) variation of injected reactive power to the grid, (c) variations of injected active power to the grid, (d) i_q component of the injected current to the grid, and (e) i_d component of the injected current to the grid.

5. Conclusions

The grid-connected performance of a single-shaft MTG system has been evaluated in this article. The mathematical modeling of the individual components of the MTG system has been presented. The detailed simulation model of the MTG system is developed using SimPowerSystems library of the MATLAB. The simulation results demonstrate the robustness of the controllers in maintaining the active power output constant during both unbalance and polluted-grid voltage conditions. The developed model of the MTG system is a useful tool for studying and accurately analyzing most of the electrical phenomena that occur when a microturbine is connected to the grid. The simulation results show that the developed model of the MTG system has the ability to adjust the output depending on the commanded power within the MTG system rating.

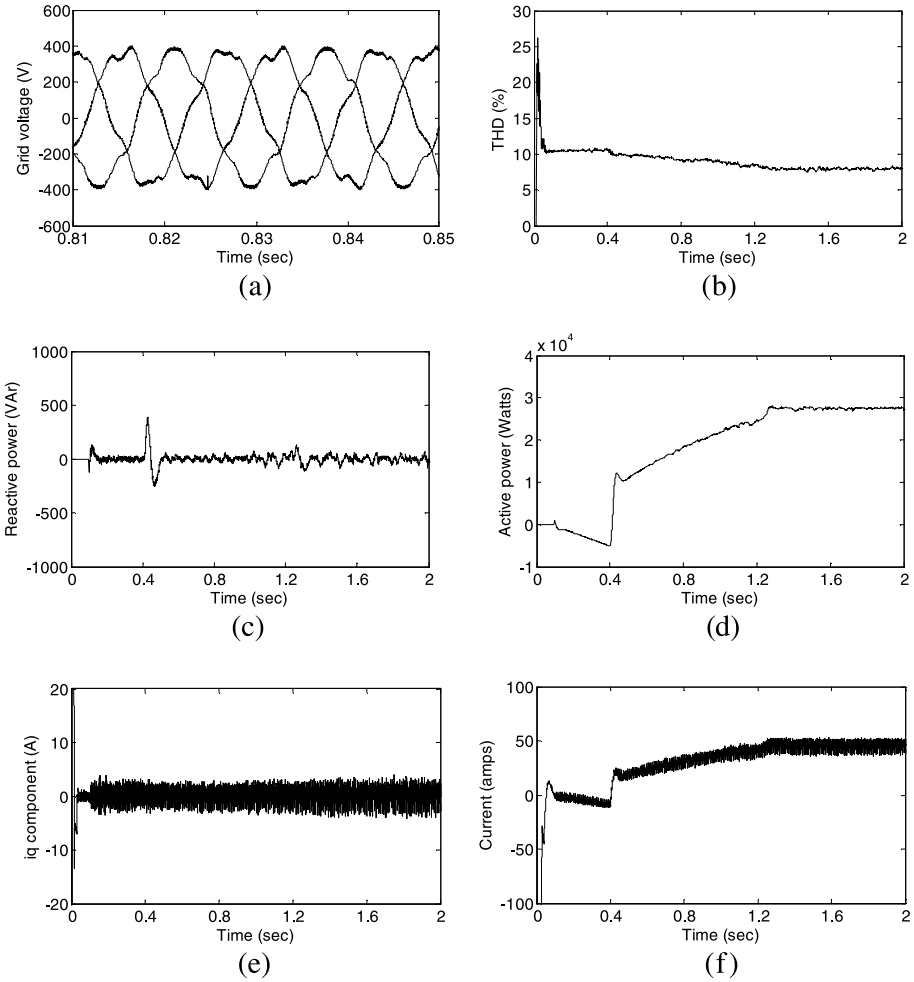

Figure 13. Response of MTG system for polluted-grid voltage: (a) polluted-phase voltage of the grid, (b) variation of the THD in percentage, (c) variation of injected reactive power to the grid, (d) variations in injected active power to the grid, (e) i_q component of the injected current to the grid, and (f) i_d component of the injected current to the grid.

References

1. Scott, W. G., "Microturbine generators for distribution systems," *IEEE Ind. Appl. Mag.*, Vol. 4, No. 3, pp. 57–62, 1998.
2. Barker, P. P., and De Mello, R. W., "Determining the impact of distributed generation on power systems: Part 1—radial distribution systems," *Proc. IEEE Power Eng. Soc. Summer Mtg.* Vol. 3, pp. 1645–1656, 2000.
3. Blaabjerg, F., Chen, Z., and Kjaer, S. B., "Power electronics as efficient interface in dispersed power generation systems," *IEEE Trans. Power Electron.*, Vol. 19, No. 5, pp. 1184–1193, 2004.
4. Al-Hinai, A., and Feliachi, A., "Dynamic model of microturbine used as a distributed generator," *Proceedings of the 34th South Eastern Symposium on System Theory*, Huntsville, AL, pp. 209–213, 18–19 March 2002.

5. Guda, S. R., Wang, C., and Nehrir, M. H., "Modeling of microturbine power generation systems," *J. Elect. Power Syst. Compon.*, Vol. 34, pp. 1027–1041, 10–12 April 2006.
6. Gaonkar, D. N., and Patel, R. N., "Modeling and simulation of microturbine based distributed generation system," *Proceedings of the IEEE Power India Conference*, New Delhi, India, pp. 256–260, 2006.
7. Rowen, W. I., "Simplified mathematical representations of heavy duty gas turbines," *ASME Trans. J. Eng. Power*, Vol. 105, No. 4, pp. 865–869, 1983.
8. Lasseter, R., "Dynamic models for micro-turbines and fuel cells," *Proc. IEEE PES Summer Mtg.*, Vol. 2, pp. 761–766, 2001.
9. Nikkhajoei, H., and Iravani, R., "A matrix converter based microturbine distributed generation system," *IEEE Trans. Power Delivery*, Vol. 20, No. 3, pp. 2182–2192, 2005.
10. Nikkhajoei, H., and Iravani, R., "Electromagnetic transients of a micro-turbine based distributed generation system," *Proceedings of the International Conference on Power Systems Transients (IPST'05)*, Montreal, Canada, 19–23 June 2004.
11. Jurado, F., and Cano, A., "Use of ARX algorithms for modeling micro-turbines on the distribution feeder," *IEE Proc. Generat. Transm. Distrib.*, Vol. 151, No. 2, pp. 232–238, 2004.
12. Fethi, O., Dessaint, L. A., and Al-Haddad, K., "Modeling and simulation of the electric part of a grid connected micro turbine," *Proc. IEEE PES General Mtg.*, Vol. 2, pp. 2212–2219, 2004.
13. Azmy, A. M., and Erlich, I., "Dynamic simulation of fuel cells and microturbines integrated with a multi-machine network," *Proceedings of the IEEE Bologna Power Tech Conference*, Bologna, Italy, 23–26 June 2003.
14. Hajagos, L. M., and Berube, G. R., "Utility experience with gas turbine testing and modelling," *Proc. IEEE PES Winter Meeting*, Vol. 2, pp. 671–677, 2001.
15. Hannet, N., and Khan, A., "Combustion turbine dynamic model validation from tests," *IEEE Trans. Power Syst.*, Vol. 8, No. 1, pp. 152–158, 1993.
16. Pillai, P., and Krishnan, R., "Modeling, simulation, and analysis of permanent-magnet motor drives, part I: The permanent-magnet synchronous motor drive," *IEEE Trans. Ind. Appl.*, Vol. 25, No. 2, pp. 265–273, 1989.
17. Urasaki, N., Senjyu, T., Uezato, K., Funabashi, T., and Fujita, H., "High efficiency drive for micro-turbine generator based on current phase and revolving speed optimization," *Proc. IEEE Int. Conf. Power Electron. Drive Syst. (PEDS)*, Vol. 1, pp. 737–742, 2003.
18. Morimoto, S., Sanada, M., and Takeda, Y., "Wide speed operation of interior permanent magnet synchronous motors with high performance current regulator," *IEEE Trans. Ind. Appl.*, Vol. 30, pp. 920–926, July/August 1994.
19. Yinger, R. J., "Behavior of capston and Honeywell microturbine generators during load changes," CERTS Consultancy Report LBNL-49095, 2004.
20. IEEE Std. 1547-2003, "IEEE standard for interconnecting distributed resources with electric power systems," 2003.